CHINESE OPTICS LETTERS

Vol. 21, No. 10 | October 2023

Slotless dispersion-flattened waveguides with more than five zero-dispersion wavelengths

Jialang Zhang (张家琅)[1], Siyuan Zhang (张思远)[1], Junna Yao (姚俊娜)[1], Xinhua Jiang (江新华)[1], Anting Wang (王安廷)[1*], and Qiwen Zhan (詹其文)[2]

[1] Department of Optics and Optical Engineering, University of Science and Technology of China, Hefei 230026, China

[2] School of Optical-Electrical and Computer Engineering, University of Shanghai for Science and Technology, Shanghai 200093, China

*Corresponding author: atwang@ustc.edu.cn

Received April 2, 2023 | Accepted May 31, 2023 | Posted Online September 28, 2023

We propose a new type of dispersion-flattened waveguide without a slot-assisted structure that can obtain an ultra-flat group velocity dispersion profile with five or six zero-dispersion wavelengths in the mid-infrared region. The dispersion profile becomes less sensitive to the waveguide dimensions due to the absence of the slot-assisted structure, making waveguide fabrication more friendly. The dispersion profile varies between −0.472 and 0.365 ps/(nm · km) over a 2665 nm bandwidth from 2885 nm to 5550 nm with a flatness of 3183.99 nm^2 · km/ps. Two different combinations of materials are demonstrated for dispersion flattening of the proposed waveguide structures. We also provide design guidance for the proposed waveguide structures with other combinations of materials.

Keywords: integrated optical devices; waveguides; dispersion.
DOI: 10.3788/COL202321.101302

1. Introduction

Chromatic dispersion is a key property of integrated waveguides that significantly affects the temporal waveform shaping and the spectral evolution of optical pulses[1]. In nonlinear optics, low dispersion over a wide spectral range can reduce the phase mismatch among interactive optical waves, thereby increasing the nonlinear efficiency and conversion bandwidth. Thus, the generation of broadband and flat dispersion profiles in integrated waveguides, also known as dispersion flattening, has attracted much interest from researchers in recent years. Dispersion flattening can enhance nonlinear processes and has been widely used for supercontinuum generation[2–7], frequency comb generation[8–10], parametric amplification[11], and ultrafast pulse manipulation[12].

However, dispersion flattening in integrated waveguides is extremely difficult because the dominant waveguide dispersion is difficult to compensate effectively for the material dispersion over a wide bandwidth[13–16]. In order to obtain a flat dispersion profile, Zhang *et al.* proposed slot-assisted silicon waveguides that utilize the coupling of strip and slot modes to generate extra dispersion for compensating the original waveguide and material dispersion[17,18]. This dispersion tailoring method can improve the dispersion flatness up to several tens of times and has been used for different polarization states[19] and various material platforms[5–8,20]. Nevertheless, the slot thickness of slot-assisted waveguides is highly sensitive to the dispersion profile, and even a change of a few nanometers can cause a large variation of the dispersion profile, which makes the fabrication of slot-assisted waveguides extremely difficult[5–8,17–20]. To make the fabrication more friendly, Guo *et al.* proposed bilayer waveguides without slot-assisted structures for dispersion flattening[21]. The removal of the slot-assisted structure simplifies the waveguide parameters from four to three and makes material selection more flexible. The bilayer waveguide structure has been used in various nonlinear applications[6,9-12,22-24]. Although the bilayer waveguide makes fabrication easier, the flatness of the dispersion profile is rarely improved. In 2019, Guo *et al.* proposed a mixed waveguide that consists of a classical slot-assisted waveguide and a slab layer beneath it to obtain an ultraflat dispersion profile[25]. In the dispersion tailoring region, the coupling of the quasi-TM and slot modes produces a mode-crossing point at the short wavelength, while the coupling of the quasi-TM and slab modes produces another mode-crossing point at the long wavelength. An ultraflat dispersion profile with five or six zero-dispersion wavelengths (ZDWs) can be produced by carefully adapting the waveguide parameters. However, due to the utilization of the slot-assisted structure, even a nanometer change in the slot thickness can cause a huge change in the dispersion profile. In addition, the complex waveguide structure makes fabrication very challenging.

In this Letter, we propose a new type of dispersion-flattened waveguide without the slot-assisted structure, where two different combinations of materials are used to produce ultraflat

Table 1. Comparison of Dispersion-Flattened Waveguides without the Slot-Assisted Structures in Recent Work.

Year	ZDW	Dispersion (ps/(nm·km))	Wavelength (nm)	Flatness (nm^2·km/ps)
2016[21]	4	−15.87 to 11.34	1520–2320	29.40
2016[21]	4	−4.73 to 5.69	1660–3290	156.73
2018[9]	4	−16 to 32	3500–10,000	135.42
2018[22]	5	−18 to 14	2600–15,500	403.13
2019[12]	4	−0.98 to 0.98	1670–2245	293.37
2021[6]	2	−24.13 to 71.17	1000–3500	26.23
2022[23]	1	0 to 27	1290–4570	121.48
2022[24]	4	−1 to 1	1810–3630	910
This work	6	−1.2 to 1.1	1980–4880	1260.87
This work	5	−0.472 to 0.365	2885–5550	3183.99

dispersion profiles with five or six ZDWs in the mid-infrared region. The obtained ultraflat dispersion profile, which has a total variation of 0.837 ps/(nm · km) over a 2665 nm bandwidth from 2885 to 5550 nm, is the flattest one among the waveguides reported so far without the slot-assisted structure. Table 1 compares the dispersion flatness and the ZDW number of dispersion-flattened waveguides without slot-assisted structures in recent work. The flatness of the dispersion profile is defined as the flat dispersion bandwidth divided by the dispersion variation within it[23].

2. Waveguide Structure and Principle of Dispersion Tailoring

As shown in Fig. 1, we add a slab layer under the bilayer waveguide core for dispersion flattening. This waveguide structure eliminates the undesired slot-assisted structure. The proposed waveguide consists of the upper strip waveguide, lower strip waveguide, slab layer, substrate, and air cladding. The lower strip waveguide has a high refractive index (n_{lower}), the upper strip waveguide has a middle refractive index (n_{upper}), the slab layer has a low refractive index (n_{slab}), and the substrate has the lowest refractive index (n_{sub}). The material refractive indices must satisfy the relationship $n_{lower} > n_{upper} > n_{slab} > n_{sub}$ to generate two mode-crossing points for dispersion flattening. The proposed waveguide can be composed of various combinations of materials, and here we provide two examples (WG1 and WG2) with different combinations of materials. In WG1, the upper strip waveguide is silicon nitride (Si_3N_4, $n \approx 1.9$), the lower strip waveguide is titanium dioxide (TiO_2, $n \approx 2.2$), the slab layer is aluminum oxide (Al_2O_3, $n \approx 1.7$), and the substrate is air. This waveguide can be fabricated by the methods described in Ref. [26]. In WG2, the upper strip waveguide is arsenic sulfide (As_2S_3, $n \approx 2.4$), the lower strip waveguide is arsenic selenide (As_2Se_3, $n \approx 2.7$), the slab layer is aluminum nitride (AlN, $n \approx 1.9$), and the substrate is calcium fluoride (CaF_2, $n \approx 1.4$). The group velocity dispersion of the guided mode is defined by

$$D = -\left(\frac{\lambda}{c}\right) \cdot \left(\frac{\partial^2 n_{\text{eff}}}{\partial \lambda^2}\right), \tag{1}$$

where λ is the wavelength and c is the speed of light in vacuum. The effective refractive index (n_{eff}) of the guided mode is obtained via the full-vectorial finite-element method. And all material dispersions are considered by the Sellmeier equations of different materials[3,27–31].

The principle of dispersion flattening in this waveguide is shown in Fig. 2. At short wavelengths, the fundamental

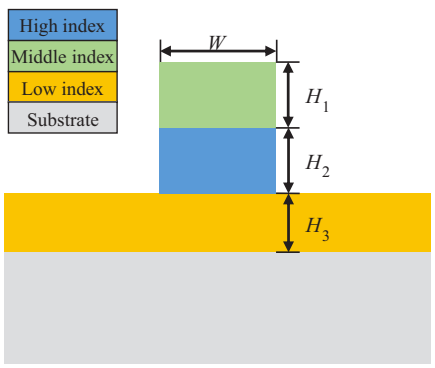

Fig. 1. Structure diagram of the dispersion-flattened waveguide.

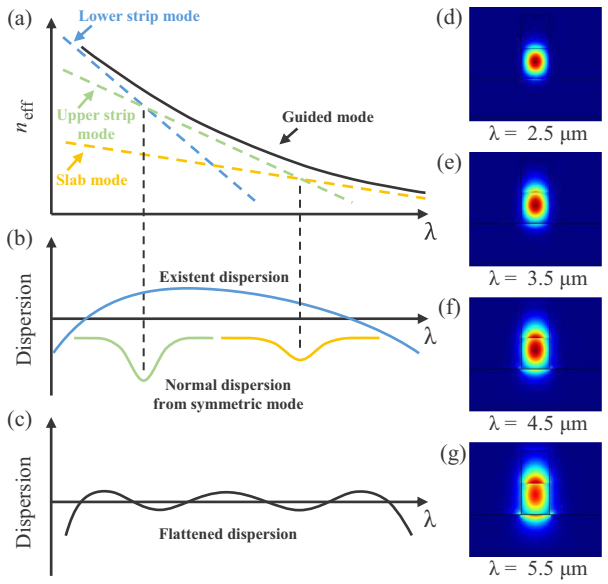

Fig. 2. (a)–(c) Principle of dispersion flattening for the proposed waveguides; optical intensity distribution of the guided mode at (d) 2500 nm; (e) 3500 nm; (f) 4500 nm; (g) 5500 nm.

quasi-TM_{00} mode is tightly confined within the lower strip waveguide. There is almost no energy leak into the upper strip waveguide or the slab layer. While the mode coupling does not happen clearly, the optical intensity distribution of the quasi-TM_{00} mode is shown in Fig. 2(d). As the wavelength increases, the n_{eff} curves of the quasi-TM_{00} mode in the lower strip waveguide and the mode in the upper strip waveguide are crossed, producing the first mode-crossing point. The mode coupling of the quasi-TM_{00} mode in the lower strip waveguide and the mode in the upper strip occurs to generate the symmetric mode. The generated symmetric mode provides additional normal dispersion ($D < 0$) to compensate for the existent dispersion, creating the first concave in the dispersion profile. Meanwhile, some energy from the quasi-TM_{00} mode leaks into the upper strip waveguide, as shown in Fig. 2(e). With a further increase in wavelength, a part of the energy of the quasi-TM_{00} mode leaks into the slab layer to form the second mode-crossing point, as shown in Fig. 2(f). The generated additional normal dispersion creates the second concave in the dispersion profile. At long wavelengths, more energy leaks into the slab layer, and the substrate until the guided mode is cut off, as shown in Fig. 2(g). As illustrated in Fig. 2(b), the guided mode experiences two mode crossings in the dispersion tailor region. The location of mode-crossing wavelengths and the strength of the mode coupling can be controlled by changing the parameters of the waveguide. As shown in Fig. 2(c), when the generated additional dispersion compensates well for the existing dispersion, it is possible to obtain an ultraflat dispersion profile with six ZDWs.

3. Results of Dispersion Tailoring

For WG1, the optimized parameters of the waveguide are $W = 1332$ nm, $H_1 = 1450$ nm, $H_2 = 938$ nm, and $H_3 = 1655$ nm. As shown in Fig. 3(a), the obtained dispersion profile varies between -1.2 and $1.1\,\text{ps}/(\text{nm}\cdot\text{km})$ from 1980 to 4880 nm with six ZDWs located at 2025, 2351, 2968, 3690, 4397, and 4798 nm, respectively. The flatness of the dispersion profile is $1260.87\,\text{nm}^2\cdot\text{km/ps}$. The materials of the strip waveguide (including the upper and lower strip waveguides) in WG1

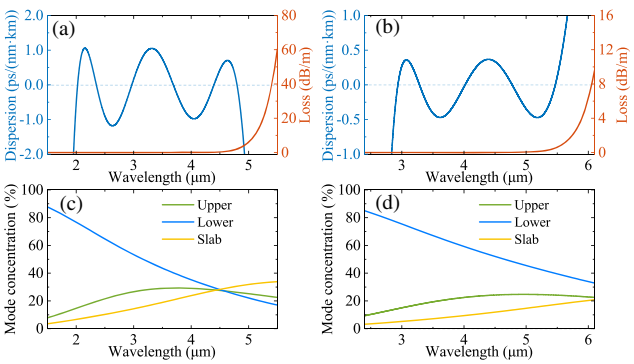

Fig. 3. Ultraflat dispersion and confinement loss of the guided mode of (a) WG1 and (b) WG2; mode concentration in upper strip, lower strip, and slab layer of (c) WG1 and (d) WG2.

and the bilayer waveguide proposed in Ref. [21] are the same. In contrast to the bilayer waveguide, the WG1 dispersion profile's flatness increases from 156.73 to $1260.87\,\text{nm}^2\cdot\text{km/ps}$, and its ZDWs also increase from four to six. For WG2, the optimized parameters of the waveguide are $W = 1150$ nm, $H_1 = 1333$ nm, $H_2 = 1272$ nm, and $H_3 = 1537$ nm. Figure 3(b) clearly shows that the dispersion profile varies from -0.472 to $0.365\,\text{ps}/(\text{nm}\cdot\text{km})$ over a 2665 nm bandwidth from 2885 to 5550 nm, with five ZDWs located at 2936, 3283, 4018, 4775, and 5469 nm, respectively. The flatness of the dispersion profile in the slotless waveguide is $3183.99\,\text{nm}^2\cdot\text{km/ps}$, which is much higher than the previous work without the slot-assisted structure, as shown in Table 1. The anomalous dispersion at long wavelengths brought by the material dispersion of the substrate reduces the ZDWs from six to five. The confinement loss of the guided mode is defined by[32]

$$\text{CL}(\text{dB/m}) = 40\pi \times \frac{\text{Im}(n_{\text{eff}})}{\lambda \ln 10}, \tag{2}$$

where $\text{Im}(n_{\text{eff}})$ represents the imaginary part of the effective mode refractive index, and λ is the wavelength in vacuum. The confinement losses of the guided mode of WG1 and WG2 are shown by the orange line in Figs. 3(a) and 3(b), respectively. The mode concentration percentages in the upper strip, lower strip, and slab layer of WG1 and WG2 are shown in Figs. 3(c) and 3(d), respectively.

In order to obtain a flattened dispersion profile in the proposed waveguide structures with other combinations of materials, Fig. 4 provides guidance for designers. Since WG1 is not affected by the material dispersion of the substrate at long wavelengths and can provide a better understanding of the dispersion tailoring process, we use WG1 as the guidance case. Figure 4 shows the variations of the dispersion profile when each waveguide parameter is changed around the optimum values shown in Fig. 3(a) by 1% every time, with the other parameters remaining constant. As shown in Fig. 4(a), the dispersion at long wavelengths is more sensitive to the waveguide width, and the increase of W can increase the slope of the dispersion profile. The effect of the upper strip waveguide height on dispersion is presented in Fig. 4(b). The parameter H_1 can control the coupling strength of the first mode-crossing point. Increasing H_1 can produce a more normal dispersion at the first mode-crossing point, making the dispersion profile more normal at short wavelengths. Figure 4(c) illustrates the influence of the lower waveguide height on the dispersion. The dispersion at short wavelengths is more sensitive to H_2, and an increase in H_2 can decrease the slope of the dispersion profile, which is the opposite of W. The proper variation of W and H can control the rise or fall of the dispersion curve while keeping the flatness constant. The influence of the slab layer height on the dispersion is illustrated in Fig. 4(d). The coupling strength at the second mode-crossing point can be controlled by H_3, and increasing H_3 can make the dispersion at long wavelengths more normal. By slightly controlling H_1 and H_3, the generated additional dispersion can compensate well for the existent one to obtain

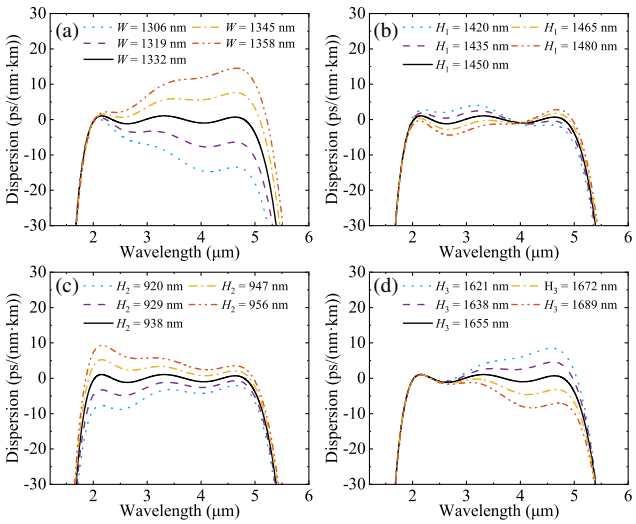

Fig. 4. Dispersion profile of WG1 with different structural parameters changed by 1% each time around the optimum values. (a) Different W, (b) different H_1, (c) different H_2, and (d) different H_3.

an ultraflat dispersion profile. It can be seen from Fig. 4 that the proposed waveguide has a better fabrication tolerance compared to the slot-assisted waveguide.

The mode field overlap factor significantly affects the nonlinear conversion efficiency in broadband nonlinear applications[33]. The mode field overlap is defined by

$$\eta = \frac{\left| \iint E_1(\lambda_1) E_2^*(\lambda_2) \mathrm{d}S \right|^2}{\iint |E_1(\lambda_1)|^2 \mathrm{d}S \iint |E_2(\lambda_2)|^2 \mathrm{d}S}, \tag{3}$$

where $E_1(\lambda_1)$ and $E_2(\lambda_2)$ are the mode profiles of the electric field at λ_1 and λ_2, respectively. Figure 5(a) shows the mode overlap factor between different wavelengths of the guided mode in WG1, where one wavelength is located at 3300 nm. The mode

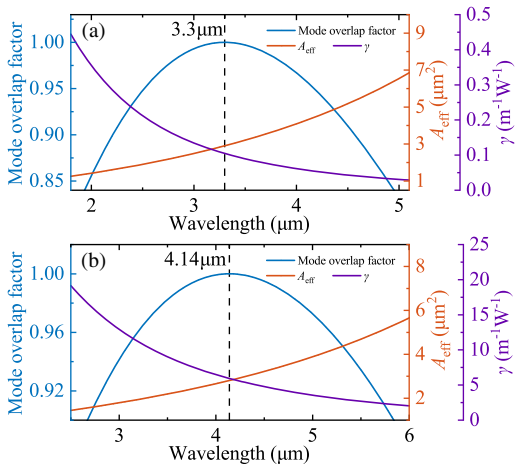

Fig. 5. (a) Mode overlap factor with one mode located at 3300 nm, A_{eff}, and γ of WG1; (b) mode overlap factor with one mode located at 4140 nm, A_{eff}, and γ of WG2.

overlap factor is better than 0.85 over the entire flat dispersion region. The mode overlap factor in WG2 with one mode located at 4140 nm is presented in Fig. 5(b). The mode overlap factor is better than 0.93 over the entire flat dispersion region. The effective mode area (A_{eff}) of the guided mode is defined by[1]

$$A_{\mathrm{eff}} = \frac{\left(\iint_{-\infty}^{\infty} |E(x,y)|^2 \mathrm{d}x\mathrm{d}y \right)^2}{\iint_{-\infty}^{\infty} |E(x,y)|^4 \mathrm{d}x\mathrm{d}y}, \tag{4}$$

where $E(x, y)$ is the mode profile of the field. The nonlinear coefficient (γ) of the guided mode is defined by[1]

$$\gamma = \frac{2\pi n_2}{\lambda A_{\mathrm{eff}}}, \tag{5}$$

where λ is the wavelength in vacuum and n_2 is the nonlinear refractive index. The orange and purple lines in Fig. 5 indicate the A_{eff} and γ of the guided mode, respectively. Due to the high mode overlap factor, the mode field mismatch in the proposed waveguides has a weak effect on broadband nonlinear processes.

4. Conclusions

In conclusion, we propose a new dispersion-flattened waveguide that can generate an ultraflat dispersion profile with five or six ZDWs without the slot-assisted structure. The removal of the thin slot-assisted structure improves the fabrication tolerance. The dispersion profile only varies by 0.837 ps/(nm · km) over a bandwidth of 2665 nm. The flatness of the obtained dispersion profile is 3183.99 nm^2 · km/ps. Fewer waveguide parameters are required to achieve an ultraflat dispersion profile with six ZDWs. Broadband dispersion flattening in the mid-infrared region is realized in the proposed waveguides. This dispersion flattening methodology can be used in the proposed waveguide structures with other combinations of materials to obtain flat dispersion.

Acknowledgement

This work was supported by the National Key Research and Development Program of China (No. 2020YFB2205802).

References

1. G. P. Agrawal, *Nonlinear Fiber Optics*, 5th ed. (Academic, 1981).
2. L. Zhang, Y. Yan, Y. Yue, Q. Lin, O. Painter, R. G. Beausoleil, and A. E. Willner, "On-chip two-octave supercontinuum generation by enhancing self-steepening of optical pulses," Opt. Express **19**, 11584 (2011).
3. L. Zhang, A. M. Agarwal, L. C. Kimerling, and J. Michel, "Nonlinear Group IV photonics based on silicon and germanium: from near-infrared to mid-infrared," Nanophotonics **3**, 247 (2013).
4. S. Roy and F. Biancalana, "Formation of quartic solitons and a localized continuum in silicon-based slot waveguides," Phys. Rev. A **87**, 025801 (2013).
5. Y. X. Fang, C. J. Bao, Z. Wang, B. Liu, L. Zhang, X. Han, Y. X. He, H. Huang, Y. X. Ren, Z. Q. Pan, and Y. Yue, "Three-octave supercontinuum generation using SiO_2 cladded Si_3N_4 slot waveguide with all-normal dispersion," J. Light. Technol. **38**, 3431 (2020).

6. Z. J. Hu, L. J. Xu, J. Wang, Y. K. Zhai, and L. Zhang, "Flattened 2.5-octave supercontinuum in a silicon nitride waveguide pumped with picosecond pulses," IEEE J. Quantum Electron. **57**, 1 (2021).
7. S. Fatema, M. B. Mia, and S. Kim, "Multiple mode couplings in a waveguide array for broadband near-zero dispersion and supercontinuum generation," J. Light. Technol. **39**, 216 (2021).
8. J. Wang, Y. H. Guo, H. N. Liu, L. C. Kimerling, J. Michel, A. M. Agarwal, G. F. Li, and L. Zhang, "Robust cavity soliton formation with hybrid dispersion," Photonics Res. **6**, 647 (2018).
9. Y. H. Guo, J. Wang, Z. H. Han, K. Wada, L. C. Kimerling, A. M. Agarwal, J. Michel, Z. Zheng, G. F. Li, and L. Zhang, "Power-efficient generation of two-octave mid-IR frequency combs in a germanium microresonator," Nanophotonics **7**, 1461 (2018).
10. J. F. Rong, Y. W. Ma, M. Xu, and H. Yang, "Interactions of the second-order solitons with an external probe pulse in the optical event horizon," Chin. Opt. Lett. **20**, 111901 (2022).
11. M. H. Yang, L. J. Xu, J. Wang, H. N. Liu, X. Y. Zhou, G. F. Li, and L. Zhang, "An octave-spanning optical parametric amplifier based on a low-dispersion silicon-rich nitride waveguide," IEEE J. Sel. Top. Quantum Electron. **24**, 8300607 (2018).
12. L. J. Xu, M. H. Yang, Y. H. Guo, H. N. Liu, G. F. Li, and L. Zhang, "Ultrafast pulse manipulation in dispersion-flattened waveguides with four zero-dispersion wavelengths," J. Light. Technol. **37**, 6174 (2019).
13. A. C. Turner, C. Manolatou, B. S. Schmidt, M. Lipson, M. A. Foster, J. E. Sharping, and A. L. Gaeta, "Tailored anomalous group-velocity dispersion in silicon channel waveguides," Opt. Express **14**, 4357 (2006).
14. J. I. Dadap, N. C. Panoiu, X. G. Chen, I. Hsieh, X. P. Liu, C. Y. Chou, E. Dulkeith, S. J. McNab, F. N. Xia, W. M. J. Green, L. Sekaric, Y. A. Vlasov, and R. M. Osgood, "Nonlinear-optical phase modification in dispersion-engineered Si photonic wires," Opt. Express **16**, 1280 (2008).
15. L. Zhang, Y. Yue, Y. Y. Xiao-Li, J. Wang, R. G. Beausoleil, and A. E. Willner, "Flat and low dispersion in highly nonlinear slot waveguides," Opt. Express **18**, 13187 (2010).
16. S. Mas, J. Caraquitena, J. V. Galán, P. Sanchis, and J. Martí, "Tailoring the dispersion behavior of silicon nanophotonic slot waveguides," Opt. Express **18**, 20839 (2010).
17. L. Zhang, Y. Yue, R. G. Beausoleil, and A. E. Willner, "Flattened dispersion in silicon slot waveguides," Opt. Express **18**, 20529 (2010).
18. L. Zhang, Q. Lin, Y. Yue, Y. Yan, R. G. Beausoleil, and A. E. Willner, "Silicon waveguide with four zero-dispersion wavelengths and its application in on-chip octave-spanning supercontinuum generation," Opt. Express **20**, 1685 (2012).
19. M. Zhu, H. J. Liu, X. F. Li, N. Huang, Q. B. Sun, J. Wen, and Z. L. Wang, "Ultrabroadband flat dispersion tailoring of dual-slot silicon waveguides," Opt. Express **20**, 15899 (2012).
20. Z. Jafari and F. Emami, "Strip/slot hybrid arsenic tri-sulfide waveguide with ultra-flat and low dispersion profile over an ultra-wide bandwidth," Opt. Lett. **38**, 3082 (2013).
21. Y. H. Guo, Z. Jafari, A. M. Agarwal, L. C. Kimerling, G. F. Li, J. Michel, and L. Zhang, "Bilayer dispersion-flattened waveguides with four zero-dispersion wavelengths," Opt. Lett. **41**, 4939 (2016).
22. Y. H. Guo, L. J. Xu, Z. Jafari, A. M. Agarwal, L. C. Kimerling, G. F. Li, J. Michel, and L. Zhang, "Two-octave dispersion flattening with five zero-dispersion wavelengths in the deep mid-IR," Proc. SPIE **10541**, 162 (2018).
23. M. L. Liu, C. W. Gu, X. N. Fan, Z. H. Li, H. M. Huang, Z. Z. Lu, and W. Zhao, "Efficient dispersion engineering for three-octave-spanning supercontinuum generation in nanophotonic waveguides," Opt. Laser Technol. **150**, 107923 (2022).
24. Y. S. Guo, Y. H. Guo, Z. Jafari, L. J. Xu, and L. Zhang, "Single-mode, single-polarization and dispersion-flattened waveguides based on silicon carbide and diamond," Opt. Laser Technol. **148**, 107692 (2022).
25. Y. H. Guo, Z. Jafari, L. J. Xu, C. J. Bao, P. C. Liao, G. F. Li, A. M. Agarwal, L. C. Kimerling, J. Michel, A. E. Willner, and L. Zhang, "Ultra-flat dispersion in an integrated waveguide with five and six zero-dispersion wavelengths for mid-infrared photonics," Photonics Res. **7**, 127 (2019).
26. M. Vlk, A. Datta, S. Alberti, G. S. Murugan, A. Aksnes, and J. Jágerská, "Free-standing tantalum pentoxide waveguides for gas sensing in the mid-infrared," Opt. Mater Express **11**, 3111 (2021).
27. K. Luke, Y. Okawachi, M. R. E. Lamont, A. L. Gaeta, and M. Lipson, "Broadband mid-infrared frequency comb generation in a Si_3N_4 microresonator," Opt. Lett. **40**, 4823 (2015).
28. E. D. Palik, *Handbook of Optical Constants of Solids* (Academic, 1998).
29. H. H. Li, "Refractive index of alkaline earth halides and its wavelength and temperature derivatives," J. Phys. Chem. Ref. Data **9**, 161 (1980).
30. D. Saha, R. S. Ajimsha, K. Rajiv, C. Mukherjee, M. Gupta, P. Misra, and L. M. Kukreja, "Spectroscopic ellipsometry characterization of amorphous and crystalline TiO_2 thin films grown by atomic layer deposition at different temperatures," Appl. Surf. Sci. **315**, 116 (2014).
31. J. Kischkat, S. Peters, B. Gruska, M. Semtsiv, M. Chashnikova, M. Klinkmüller, O. Fedosenko, S. Machulik, A. Aleksandrova, G. Monastyrskyi, Y. Flores, and W. T. Masselink, "Mid-infrared optical properties of thin films of aluminum oxide, titanium dioxide, silicon dioxide, aluminum nitride, and silicon nitride," Appl. Opt. **51**, 6789 (2012).
32. M. Meng, D. X. Yan, M. X. Cao, X. J. Li, G. H. Qiu, and J. J. Li, "Design of negative curvature fiber carrying multiorbital angular momentum modes for terahertz wave transmission," Results Phys. **29**, 104766 (2021).
33. Q. Lin, O. J. Painter, and G. P. Agrawal, "Nonlinear optical phenomena in silicon waveguides: modeling and applications," Opt. Express **15**, 16604 (2007).